Author's Version

Investigation of CMAS Resistance of Sacrificial Suspension Sprayed Alumina Topcoats on EB-PVD 7YSZ Layers

by

Christoph Mikulla[1], Ravisankar Naraparaju[1], Uwe Schulz[1], Filofteia-Laura Toma[2], Maria Barbosa[2,3], Lars Steinberg[3], Christoph Leyens[2,3]

[1)] German Aerospace Center (DLR), Institute of Materials Research, Cologne, Germany
[2)] Fraunhofer Institute for Material and Beam Technology (IWS), Dresden, Germany
[3)] Technische Universität Dresden (TUD), Institute of Materials Science, Dresden, Germany

Journal of Thermal Spraying Technology (2019)
https://doi.org/10.1007/s11666-019-00951-4

Investigation of CMAS Resistance of Sacrificial Suspension Sprayed Alumina Topcoats on EB-PVD 7YSZ Layers

Christoph Mikulla*, Ravisankar Naraparaju, Uwe Schulz
German Aerospace Center (DLR), Institute of Materials Research, Cologne, Germany
**)* *christoph.mikulla@dlr.de*

Filofteia-Laura Toma[1,]*, Maria Barbosa[1,2], Lars Steinberg[2], Christoph Leyens[1,2]
[1)] Fraunhofer Institute for Material and Beam Technology (IWS), Dresden, Germany
[2)] Technische Universität Dresden (TUD), Institute of Materials Science, Dresden, Germany
**)* *filofteia-laura.toma@iws.fraunhofer.de*

Abstract

Molten calcium-magnesium-aluminum-silicate (CMAS) mineral particles cause significant degradation of thermal barrier coatings (TBCs) in aero-engines. One approach to protect the TBC coating against the CMAS attack is the application of a sacrificial coating on top of the TBC coating. In this work sacrificial Al_2O_3 coatings were deposited on top of EB-PVD 7YSZ layers using suspension plasma spraying (SPS) and suspension high velocity oxy-fuel spraying (SHVOF), in order to produce sacrificial topcoats with two different microstructures and porosity levels. The coating systems were tested under CMAS attack with one natural volcanic ash and two artificial CMAS powders by conducting infiltration tests at 1250 °C in the time intervals between 5min and 10h.
While the porous SPS-coatings offer limited resistance against CMAS infiltration, the dense SHVOF-coatings show promising CMAS sealing behavior. Amongst the formed reaction products, only Mg-Al-Fe spinel acted as an efficient barrier against CMAS infiltration. However, formation of uniform spinel layers strongly depends on the pore morphology and the CMAS chemistry. Overall, it was found that the porosity and morphology of suspension sprayed alumina topcoats and the chemical composition of the deposit strongly influence the CMAS infiltration and reaction kinetics.

Keywords: 7YSZ, Al_2O_3, CMAS, EB-PVD, sacrificial coating, suspension spraying, thermal barrier coatings

Introduction

In modern airplane engines and gas turbines, thermal barrier coatings (TBCs) are deposited on various components (like turbine blades, vanes, combustion liners) in the high temperature section, in order to increase the operating temperature and hence to improve the efficiency and power of the engine. 7 wt.-% Y_2O_3 stabilized ZrO_2 (7YSZ) ceramic is used as state-of-the-art TBC material [1-3]. It is typically deposited either by electron beam physical vapor deposition (EB-PVD) or by atmospheric plasma spraying (APS) [4]. These processes create a porous microstructure with low thermal conductivity and high resistance against thermal cyclic stresses that occur due to thermal expansion. In operating conditions, the TBC coatings undergo severe degradation by interaction with molten calcium-magnesium-aluminum-silicate (CMAS) minerals that are typically found in desert sands or volcanic ashes [5-7]. After infiltration of the CMAS into the porous coating, chemical reactions and phase transformations can cause residual stresses, cracks and spallation,

J Therm Spray Tech; Mikulla et. al. 2019, https://doi.org/10.1007/s11666-019-00951-4

strongly reducing the life-time of the component. At the same time, CMAS can be an erosive medium where TBCs undergo severe mechanical degradation. The state-of-the art TBC material 7YSZ offers only limited resistance to the CMAS attack. Intense research has been and still is done in the last decades to solve this issue.
Another factor influencing the CMAS-induced degradation of TBCs is the type of CMAS itself. The desert/runway sand and volcanic ashes damaging the TBC in in-service turbines differ in their chemical composition, viscosity, melting range, degree of crystallinity or reactivity depending on their geographical origin [8-12]. The concentrations of various oxides within the CMAS can have significant influence on the TBC-CMAS interaction. In one of the recent studies [10], it was found out that presence of FeO within the CMAS influences the formation of garnet phase. In other studies it was found that CMAS containing $CaSO_4$ causes a more vigorous damage than $CaSO_4$-free deposit [7].

Different approaches, as summarized by Mohan et al. [13], have been proposed to mitigate CMAS attack of TBCs: employing an impermeable surface coating for TBCs that can act as an inert barrier between CMAS deposit and TBC; utilizing a sacrificial layer that can trap CMAS deposits through chemical interactions; surface sealing of YSZ topcoat or modifying the YSZ topcoat chemistry. Recently, novel TBCs with zirconate pyrochlores topcoats [10] received a great attention due to their promising resistance against CMAS attack. However, these novel TBCs are more susceptible to erosion than 7YSZ due to their lower toughness. One strategy against the CMAS problem is the deposition of a sacrificial layer on top of the standard 7YSZ layer. The sacrificial layer has to dispose a high reactivity with the molten CMAS and to form crystalline phases that delay further infiltration by sealing pores and gaps of the TBC [10, 14, 15]. However, these novel TBCs are more susceptible to erosion than 7YSZ due to their lower toughness. Aluminum oxide (Al_2O_3) is a promising candidate as sacrificial top-layer, due to the formation of arresting phases which offer a good CMAS resistance. Alumina has already been deposited as a CMAS resistant material on top of 7YSZ with different deposition techniques [13, 16, 17]. The most recent study [18] includes EB-PVD alumina layer. However, EB-PVD Al_2O_3-topcoats suffered locally from cracks that arise from crystallization and sintering shrinkage. As a consequence, the resistance against CMAS infiltration was insufficient due to the characteristic morphology. It was found that the microstructure, the coating density and the distribution of the porosity were critical factors for the efficiency of sacrificial layers against CMAS infiltration and degradation.

As the Al_2O_3 layer microstructure is strongly influenced by the fabrication process, new innovative coating methods are used to create the sacrificial layer with the desired morphology. Over the last years, extensive development efforts have uncovered the potential of thermal spraying with suspensions. Coating thicknesses, morphologies and properties can be varied over an extremely wide range, as presented i.e. [19-21]. Direct processing of nano- and sub-micron-sized powders is possible with suspensions, but more important is the advantage of directly using the finely dispersed ceramic oxide powders of widely varying grain size, purity, etc. currently used in the preparation of sintered technical ceramics. Suspensions can be used as feedstock for both atmospheric plasma spraying (APS) and high velocity oxy-fuel spraying (HVOF) processes.

In this work, alumina coatings were sprayed on top of EB-PVD 7YSZ TBCs layers using suspension spraying processes- suspension plasma spraying (SPS) and suspension high velocity oxy-fuel spraying (SHVOF), respectively – starting from a finely dispersed aqueous Al_2O_3 suspension. In order to evaluate the CMAS resistance of the sacrificial Al_2O_3

J Therm Spray Tech; Mikulla et. al. 2019, https://doi.org/10.1007/s11666-019-00951-4

suspension sprayed coatings, short- and long-term isothermal CMAS infiltration tests with two different types of synthesized CMAS and one natural volcanic ash were performed on the coating systems. Influence of coating microstructure on the CMAS infiltration kinetics and reaction products formation was investigated by means of scanning electron microscopy, EDX-spectroscopy and X-ray diffraction. Chemical compositional influence of CMAS on the reaction products is discussed and the potential application of the suspension spraying as CMAS-resistant sacrificial Al_2O_3 coatings is presented.

Experimental methods

Preparation of EB-PVD 7YSZ Layers

7YSZ layers (7wt.-% Y_2O_3 stabilized ZrO_2) were deposited via EB-PVD (electron beam physical vapor deposition) process at the Germany Aerospace Center (DLR) in Cologne, Germany, employing special process parameters developed previously to achieve a special "feathery" microstructure [6]. The coating process used single source evaporation with a 7YSZ ingot. The main process parameters and layer thicknesses are shown in Table 1.

Table 1: Processing parameters of 7YSZ layers deposited by EB-PVD on sintered Al_2O_3 substrates.

	7YSZ for SPS Al_2O_3	**7YSZ for SHVOF Al_2O_3**
Substrate temperature	860 – 890 °C	915 - 930 °C
Pressure	$6x10^{-3}$ mbar	
Rotation speed	30 rpm	
Beam power	65 kW	
Coating thickness	220 µm	400 µm

In order to avoid the oxidation of metal substrates during the infiltration experiments at 1250 °C, the 7YSZ was deposited on flat, 1 mm thick sintered Al_2O_3 substrates. Samples with two different 7YSZ-thicknesses of ~ 220 µm and ~ 400 µm were prepared for this study. This thickness and microstructure deviation of YSZ would not have any significant effect on the results presented here, since this work focuses only on the microstructure and infiltration/reaction kinetics of the sacrificial alumina top layer and not of the underlying 7YSZ-layer.

Suspension Spraying of Sacrificial Al_2O_3 Coatings on YSZ EB-PVD Layers

Alumina coatings with different microstructures were produced via suspension spraying at Fraunhofer IWS, Dresden, Germany. SHVOF was used to produce dense alumina coatings, whereas SPS was used to produce rather porous coatings on top of YSZ EB-PVD layers.
A commercially available Al_2O_3 raw powder (> 98 % purity, Martinswerk, Germany) with an average particle size (d_{50}) of 2.2 µm was used to obtain an aqueous suspension with 25 wt.-% solid content.
The suspensions were fed using the industrially suitable three pressurized-vessels suspension feeder developed by Fraunhofer IWS [20-22].
The Al_2O_3 suspension was internally injected in the modified combustion chamber of a HVOF Top Gun torch (8 mm diameter and 135 mm-length nozzle, GTV mbh, Germany) using ethylene as fuel gas. In the SPS process, Al_2O_3 suspension was externally injected in an APS F6 plasma gun (GTV) with 6 mm-nozzle and Ar/H_2 plasma gas mixture. Suspension

J Therm Spray Tech; Mikulla et. al. 2019, https://doi.org/10.1007/s11666-019-00951-4

sprayed coatings with thicknesses of 80 – 90 µm were deposited directly on top of the EB-PVD YSZ layers.

CMAS Deposit and Infiltration Experiments

Deposits with different chemical compositions were used for the infiltration studies: one natural volcanic ash collected from site of the Eyjafjallajökull volcano located in Iceland (named IVA) and two artificial CMAS powders (named CMAS1 and CMAS2) matching the compositions found in aero-engines operated in desert locations and already used in various other publications [5, 7].

The CMAS powders were artificially synthetized in the laboratory as described in previous studies [5]. For CMAS1, Me-nitrates (Me: Al, Ca, Mg, Fe), SiO_2 and TiO_2 powders (Merck, Germany) were synthesized by means of co-decomposition, followed by a heat treatment at 1250°C for 1 h. CMAS2, which has a higher CaO content, was fabricated by mixing CMAS1 with anhydrite $CaSO_4$ powder at room temperature.

The chemical composition, melting ranges and measured viscosities of the used deposits are given in Table 2.

Table 2: Chemical composition in mol.-% and properties of CMAS/VA including the measured viscosity values of CMAS1+CMAS2 [9] and IVA.

	Chemical composition [mol.%]								Melting range	Viscosity η at 1250°C (experimental)	Main phases
	SiO_2	CaO	MgO	Al_2O_3	FeO	TiO_2	Na_2O	K_2O			
Iceland volcanic ash (IVA)	49,7	12.5	6.	7.4	17.6	4.3	2.0	0.4	1060-1150°C	250 Pa·s	Amorphous
CMAS1 (synthetic)	41.6	24.7	12.3	11.1	8.7	1.6	-	-	1230-1250°C	6.9 Pa·s	Pyroxene + Anorthite
CMAS2 (synthetic)	37.3	32.4	11.2	9.9	7.8	1.4	-	-	1215-1245°C	4.0 Pa·s	Pyroxene + Melilite

Infiltration tests were performed by applying CMAS/VA powder with a concentration of 10 mg/cm² on top of the Al_2O_3-7YSZ double layer coating system. The samples were heated up to 1250 °C and hold in ambient air isothermally at this temperature for durations of 5 min 1, 5 and 10 hours respectively. The short-term infiltration (5 min) tests were performed in a cyclic furnace with an overall heating rate of 142 K/min and rapid cooling (quenching) to room temperature with ventilated ambient air. The long-term infiltration tests (1 to 10 h) were performed in a Netzsch box furnace with a heating and cooling rate of 10 K/min.

Al_2O_3 raw powder (same used for the preparation of the aqueous suspension prior for the spraying process) was mixed with CMAS/VA deposits in proportions of 60 wt. % CMAS/VA deposit, 40 wt. % Al_2O_3, annealed for 5h on a platinum foil and used for X-ray diffraction studies for phase identification.

Characterization Methods

The coatings were metallographically prepared and analyzed by scanning electron microscopy (SEM) (DSM ultra 55, Carl Zeiss, Germany).

Energy-dispersive spectroscopy (EDS) (Inca, Oxford Instruments, UK) was used to identify the CMAS reaction products within the coatings. The in-plane porosity of the as-deposited

J Therm Spray Tech; Mikulla et. al. 2019, https://doi.org/10.1007/s11666-019-00951-4

alumina coatings was determined by image analysis in SEM micrographs using the ImageJ software.
XRD analysis of the CMAS/VA-alumina reaction products in powder mixture, as well as of the raw powder and the as-sprayed SPS- and SHVOF-alumina coatings were carried out with a D8 Advance diffractometer with Cu-Kα radiation (Bruker AXS, Germany).
By using a powder mixture, a higher quantity of reaction products was formed (due to the higher specific contact surface area) leading to a stronger signal of the relevant peaks.

Results

Microstructures of the As-Sprayed Suspension Sprayed Al_2O_3 Coatings

Suspension sprayed alumina coatings with different microstructures were successfully deposited on columnar EB-PVD 7YSZ TBCs. The SEM micrographs of the as-sprayed coatings at two different magnifications are shown in Fig. 1.

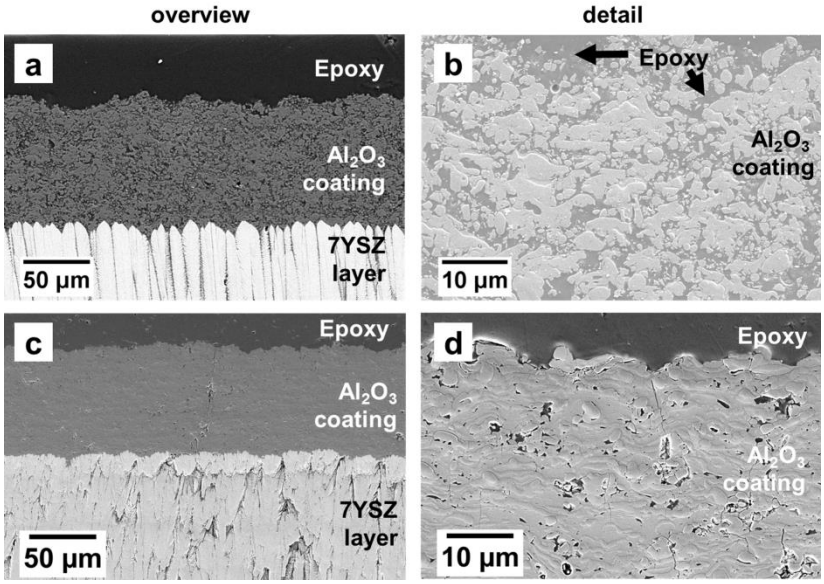

Figure 1: SEM micrographs of as-sprayed SPS-alumina (a, b) and SHVOF-alumina (c, d) on top of EB-PVD 7YSZ TBC layers.

The special “feathery” microstructures of the underlying EB-PVD 7YSZ layers have been studied elsewhere [6, 7] and are not specifically investigated in this work, as it focuses on the alumina top-layers. The deviation in the microstructure of the 7YSZ-layers that can be seen in Fig.1a and Fig. 1c, was linked to slightly different substrate temperatures and short pressure fluctuations during the 7YSZ coating process, but has no effect on the microstructure, infiltration and reaction kinetics of the alumina top-layers.
SPS-alumina coating contained a porous microstructure of well-molten particles alternating with partially molten or already cooled finely particles (Fig. 1b). The porosity of SPS coatings was estimated at around 30 %. SHVOF-alumina coatings were densely structured and contained mostly well-molten particles (Fig. 1d).
The presence of localized vertical cracks coming from the internal/relaxing stresses could be observed in the coating cross-sections and surface (Fig.2).
Additional cracks propagate horizontally from the vertical cracks between the single layers of SHOVF-coating (Fig.2a). These cracks are mainly due to the high internally thermally and relaxation stresses during spraying of the samples.

J Therm Spray Tech; Mikulla et. al. 2019, https://doi.org/10.1007/s11666-019-00951-4

The porosity of SHVOF coatings was estimated to be about 4 %. From the SEM-micrographs shown in Fig. 1 it can be observed that the fine particles of alumina anchored more intimately with YSZ layer in the case of SHVOF coatings than for SPS coatings

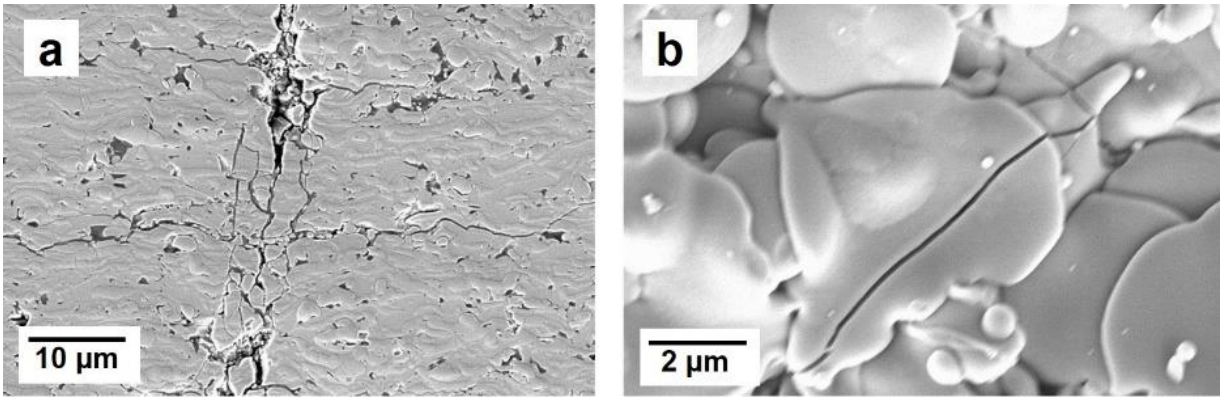

Figure 2: SEM micrographs of the localized cracks in as-sprayed SHVOF-Al_2O_3 coating in cross-section (a) and in top view (b)

The XRD patterns of the as-sprayed SPS- and SHVOF-coatings as well as of the Al_2O_3 raw powder used for the preparation of the suspension prior to the spraying process are given in Fig. 3. The raw powder consists of only corundum α-Al_2O_3. The as-sprayed SPS- and SHVOF-Al_2O_3 coatings consisted of α-Al_2O_3 and metastable γ-Al_2O_3 phases.
The unindexed peaks might originate from transient, metastable Al_2O_3 phases, due to the high cooling rates of the SHVOF-process, or from the underlying 7YSZ, as XRD-patterns of the 7YSZ layer without Al_2O_3 (not shown here) indicate strong peaks at that 2θ= 50° and 60° positions.

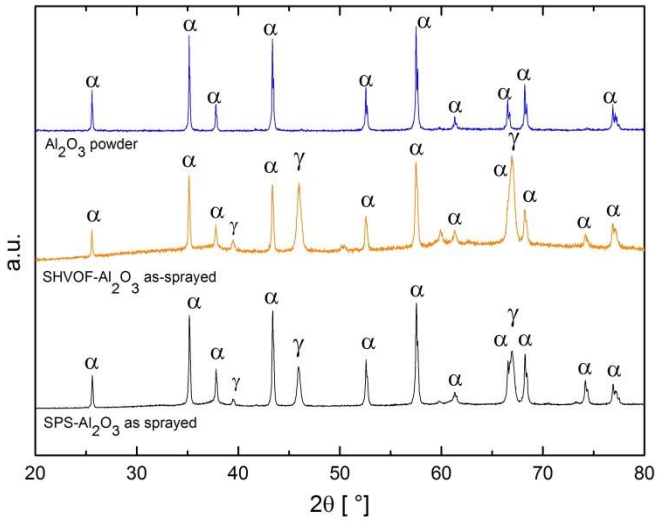

Figure 3: Normalized XRD patterns of the Al_2O_3 raw powder used for preparation of the suspension prior for the spraying process (blue pattern), as-sprayed SHVOF-(orange pattern) and SPS-Al_2O_3 coating (black pattern).

Reaction Phases in Al_2O_3-CMAS Powder Mixtures

The XRD patterns of the powder mixtures of Al_2O_3 with the three different CMAS/VA deposits after 5 h-annealing at 1250°C are given in Fig. 4.
The peaks are identified as anorthite (An) $CaAl_2Si_2O_8$, spinel (Sp) $Mg_{1-x}Al_2Fe_xO_4$, gehlenite (Ge) $Ca_2Al_2SiO_7$, pseudobrookite (Ps) $Fe_{2-x}Ti_xO_3$, diopside (Dio) $Ca(Mg, Al)(Si, Al)_2O_6$ and

J Therm Spray Tech; Mikulla et. al. 2019, https://doi.org/10.1007/s11666-019-00951-4

corundum α-Al_2O_3 (α). While the corundum, anorthite and spinel peaks are found for all three powder mixtures, gehlenite is only assigned to the Al_2O_3-CMAS2 pattern and pseudobrookite only in the Al_2O_3-IVA pattern. Diopside-peaks were found in the XRD-patterns of the Al_2O_3-CMAS1 and Al_2O_3-CMAS2 mixture. These findings are in good agreement with those published elsewhere [18].

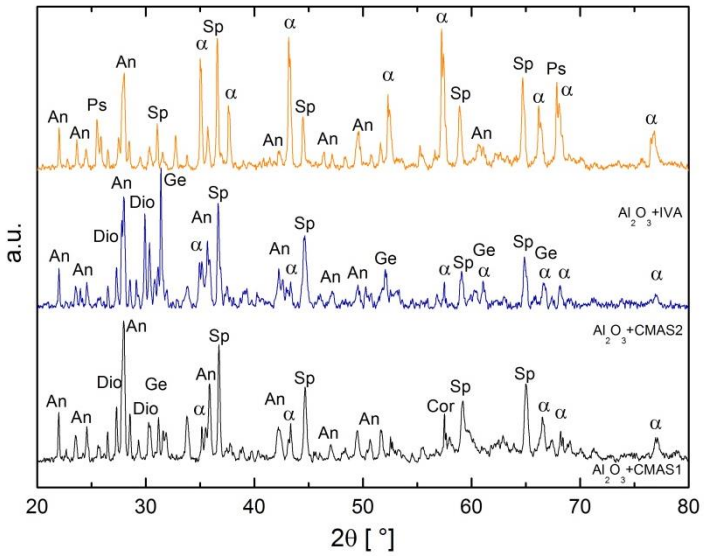

Figure 4: Normalized XRD patterns of Al_2O_3-CMAS/VA (40 wt.-% -60wt.-%) powder mixtures after 5h-annealing at 1250°C with IVA (orange pattern), CMAS1 (black pattern) and CMAS2 (blue pattern)

Microstructures of the CMAS-Infiltrated Suspension Sprayed Al_2O_3 Coatings

The results of the 5 min and 5 h infiltration tests are presented in this section with SEM micrographs and EDS measurements, representing an initial stage and a further advanced stage of the infiltration and reaction process (5 min). Additional infiltration experiments of 1 h and 10 h have been evaluated to determine the reaction layer thicknesses but are not presented here in detail.

Figures 5 to 8 show cross-sectional SEM-micrographs of the various coatings infiltrated with CMAS1, CMAS2 or IVA during 5 min and 5 h infiltration tests at 1250 °C. In each of these figures, the images a to c show overview images of the entire alumina layer, whereas the images d to f allows a detailed look at the reaction zone in high magnification.

The labels of the reaction phases in Fig. 5 to 8 were determined by combining the XRD analysis of the powder mixtures (Fig. 4), with the chemical composition of a specific phase from the EDS spot measurements (Tab. 3 - 5). These phases are explicitly described in the subsequent section.

<u>Short-Term Infiltration Test (5 min @ 1250°C)</u>

The SEM cross-sectional micrographs of the alumina coatings after 5 min of infiltration are shown in Fig. 5 for SPS coating and Fig. 6 for SHVOF coating.

The SPS-alumina coatings were found to be already infiltrated and the infiltration was mostly inhomogeneous within the coating. The depth varies between a few microns up to the entire 90 µm thick alumina coating, as shown in the micrographs (Fig. 5a-c) by the dashed lines, which implicates that the subjacent 7YSZ gets infiltrated as well.

The infiltration depth has varied with respect to the deposit chemistry. CMAS2 and IVA have shown stronger infiltration behavior – i.e. a higher fraction of the SPS coating is entirely

J Therm Spray Tech; Mikulla et. al. 2019, https://doi.org/10.1007/s11666-019-00951-4

infiltrated and the CMAS/VA has reached the subjacent 7YSZ layer (Fig. 5b and Fig. 5c). In contrast, the infiltration of CMAS1 is mostly limited to a few microns (Fig. 5a). A certain amount of CMAS residue remains on top of the coating; in case of CMAS1 and IVA around 20 µm thick CMAS residue (Fig.5a, c) is left, whereas this residue layer (Fig. 5b) is considerably thinner in CMAS2.

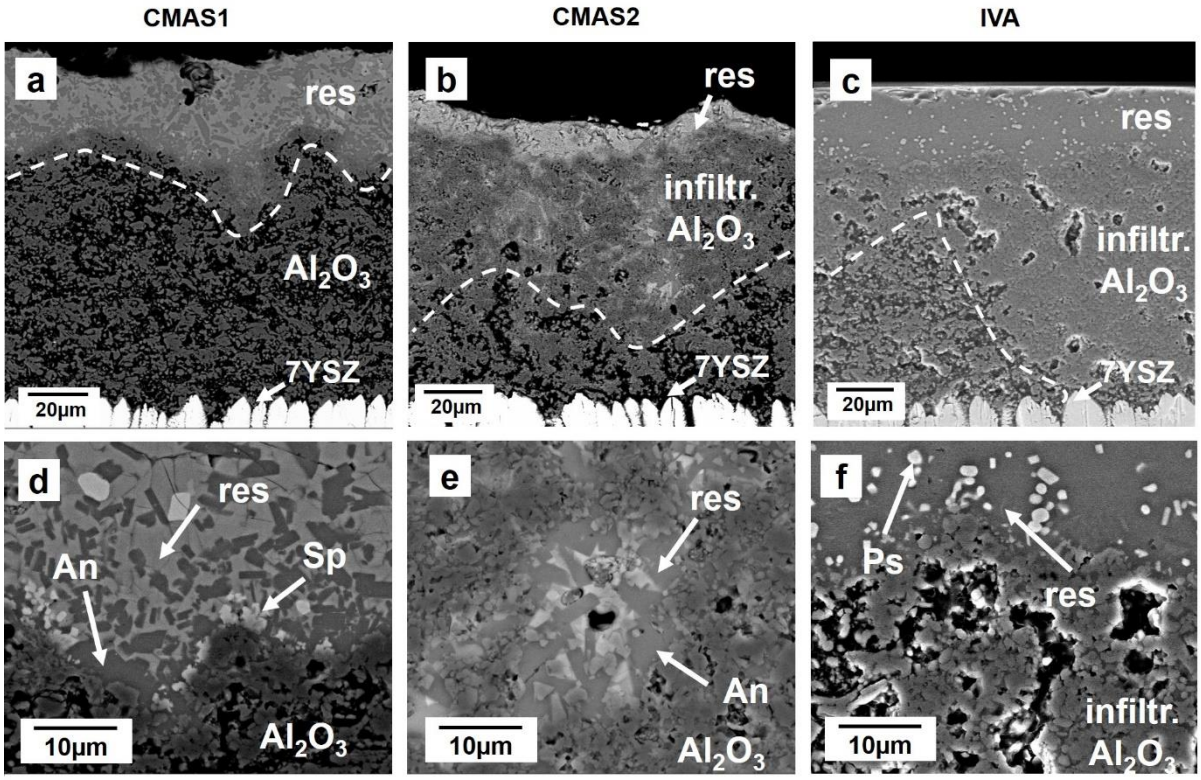

Figure 5: SEM cross-section micrographs of SPS-alumina coatings after short-term infiltration (5 min at 1250 °C) with CMAS1 (a, d), CMAS2 (b, e) and IVA (c, f), dashed lines indicate the infiltration depth, Phases: An = anorthite, Sp = spinel, Ps = pseudobrookite, res = CMAS residue

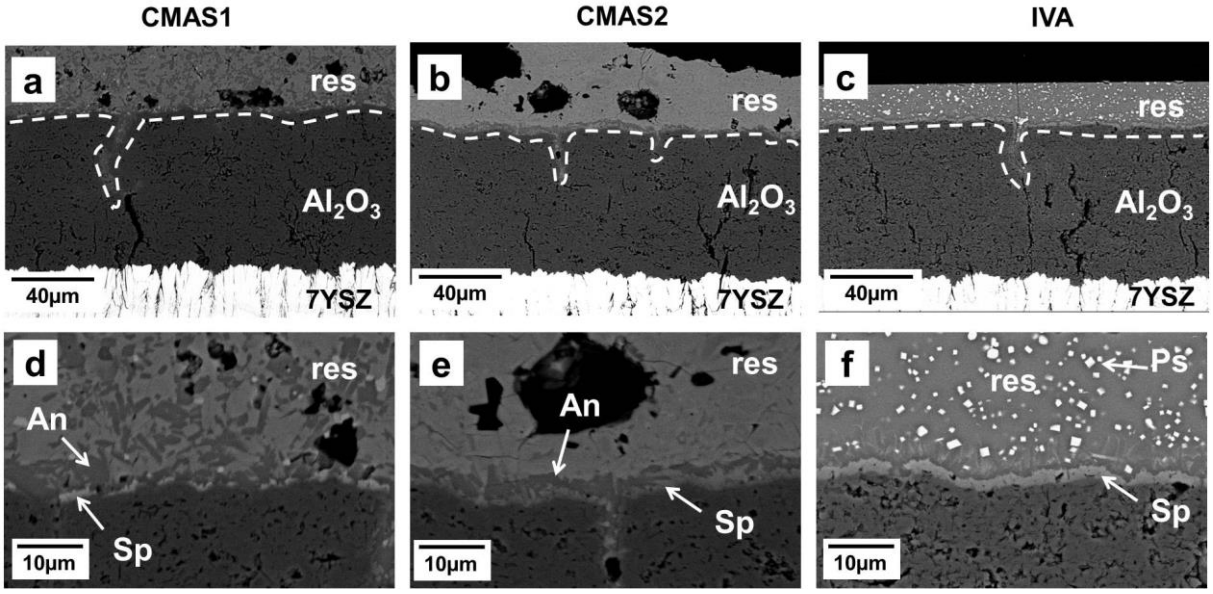

Figure 6: SEM cross-section micrographs of SHVOF-alumina coatings after short-term infiltration (5 min at 1250 °C) with CMAS1 (a, d), CMAS2 (b, e) and IVA (c, f), dashed lines indicate the infiltration depth. Phases: An = anorthite, Sp = spinel, Ps = pseudobrookite, res = CMAS residue

J Therm Spray Tech; Mikulla et. al. 2019, https://doi.org/10.1007/s11666-019-00951-4

Reduced CMAS infiltration depth was observed with all the three CMAS/VA deposits in the SHVOF alumina layer. The molten CMAS/VA has infiltrated up to a few microns depth only. In few areas, where large cracks or gaps are present, a limited infiltration could be locally observed (light grey areas). Figure 6 shows cross-sections of the SHOVF after 5 min infiltration for CMAS1 (Fig. 6a, d), CMAS2 (Fig. 6b, e) and IVA (Fig. 6c, f).

Long-Term Infiltration Test (5 h @ 1250°C)

The SEM-micrographs after 5 h infiltration are shown in Fig.7 (SPS) and Fig.8 (SHVOF). The SPS-alumina coatings are almost entirely infiltrated in case of CMAS2 and IVA (an extension to the 5 min case), which allowed the melt to infiltrate further into the subjacent 7YSZ-layer (see Fig.10). Especially, in the CMAS2 case, (Fig. 7b) the infiltration is found to be highly inhomogeneous, whereas for IVA (Fig.7, c) the SPS coating appears to be entirely infiltrated.

In case of CMAS1 (Fig. 7 a) a thick reaction layer has formed that prevents the melt from further infiltration. Considerable CMAS residue still remains above the reaction layer.

For CMAS2 and IVA, there is no formation of continuous, dense reaction layers at the CMAS/alumina interface. Instead, discrete crystals were formed which have offered zero resistance to the CMAS flow. No significant amount of residue remains on top of the coating. In case of CMAS2, small- to medium-sized crystals with a needle-like or extended structure were formed within the coating (Fig.7b, e) dissolving the as-sprayed structure. For IVA (Fig.7c, f) case, the reaction products mostly fill the gaps or have a shape and size similar to the as-sprayed alumina.

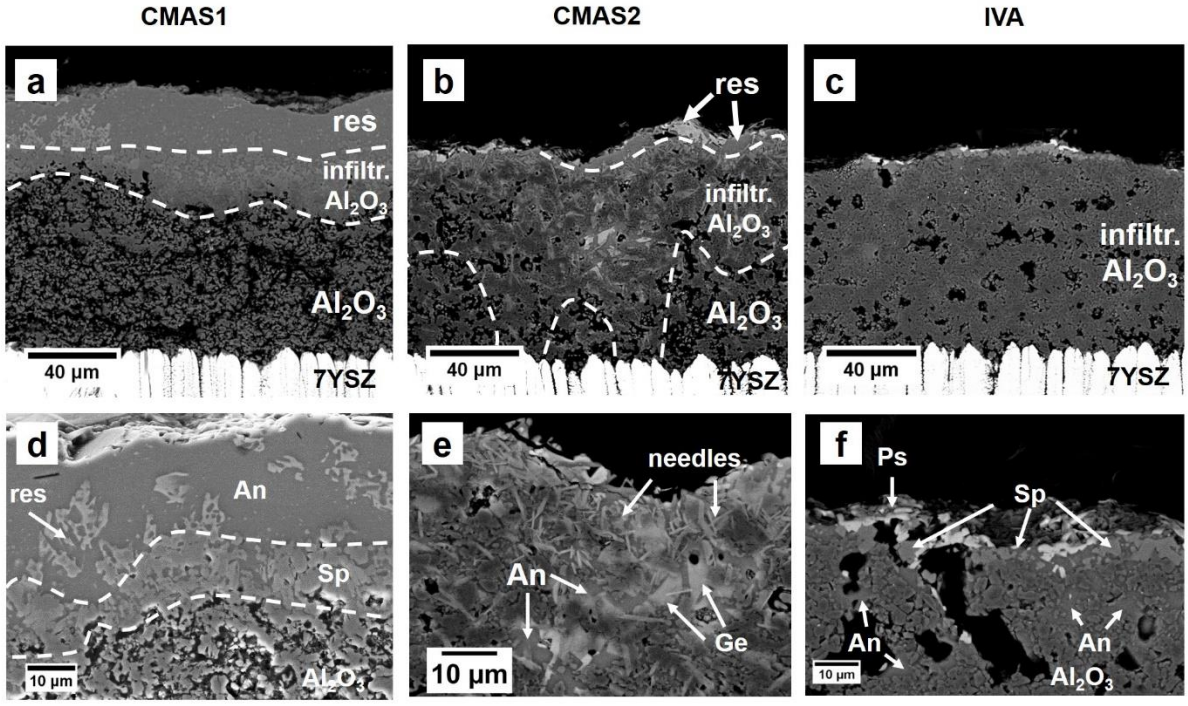

Figure 7: SEM cross-section micrographs overview of SPS-alumina coatings after long-term infiltration (5h at 1250°C) with CMAS1 (a,d), CMAS2 (b,e) and IVA (c,f), dashed lines indicate the infiltration depth Phases: An = anorthite, Sp = spinel, Ge = gehlenite,, needles = "needle-like" phase, Ps = pseudobrookite, res = CMAS residue

J Therm Spray Tech; Mikulla et. al. 2019, https://doi.org/10.1007/s11666-019-00951-4

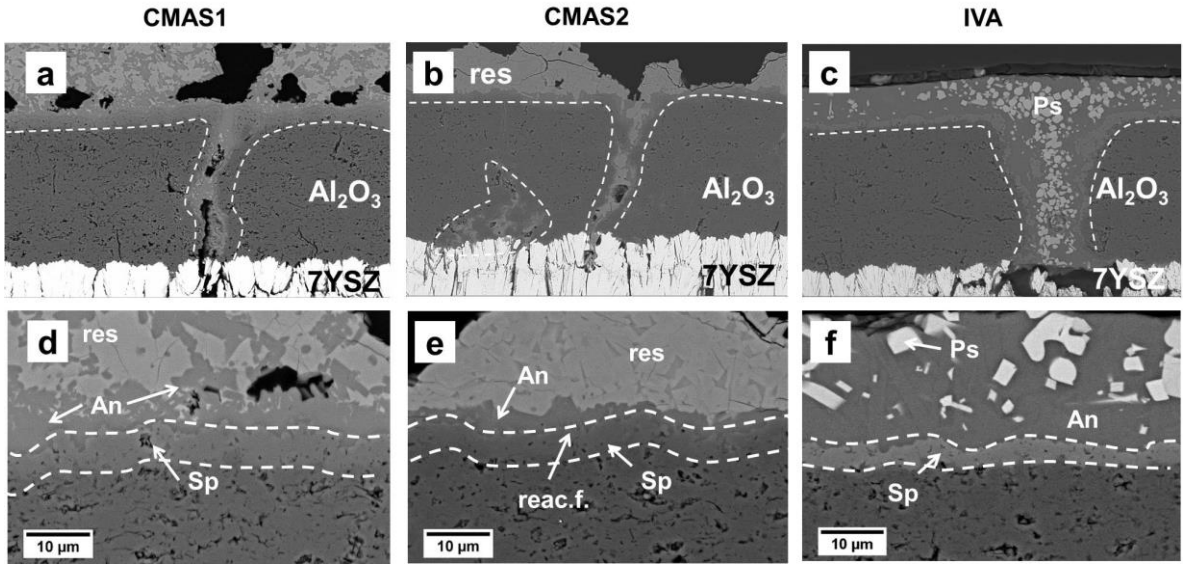

Figure 8: SEM cross-section micrograph of SHVOF-alumina coating after long-term infiltration (5h at 1250°C) with CMAS1 (a,d), CMAS2 (b,e) and IVA (c,f), dashed lines indicate the infiltration depth
Phases: An = anorthite, Sp = spinel, reac.f= reaction front, Ps = pseudobrookite, res = CMAS residue

In contrast, the SHVOF-coatings offer higher resistance to the CMAS flow. Figure 8 shows cross-sectional SEM micrographs after 5 h infiltration with CMAS1 (a, d), CMAS2 (b, e) and IVA. The crack-free areas were infiltrated only by a few microns for all three deposits used in the study. Considerable amount of CMAS/VA residue remains above the reaction layer. The SHVOF-alumina has formed a reaction layer which predominantly contains (Fe, Mg) Al spinel oxide that hindered the CMAS from further infiltration. In the regions of vertical cracks CMAS has infiltrated deeply, reaching the surface of the 7YSZ-layer (Fig. 10). Moreover, a local dissolution of the coating and formation of new reaction products at the crack interface are observed. These new products induced a broadening of the crack gap, too. Occasionally, as seen in Fig. 8b, localized pockets within the SHVOF-coating are filled with CMAS residue, although no direct crack leading from the surface to that pocket was seen in the SEM-micrograph. This might occur, as some cracks are inclined and can, par consequence, not be visible in a 2D-cross-sectional image.

The needle-like structured phase is only found in the SPS-coating with CMAS2 after long term infiltration tests. Its formation seems to be influenced by the cooling conditions during the experiment. Therefore, another SPS-alumina sample with the same amount of CMAS 2 was infiltrated for 5h at 1250°C but quenched immediately instead of slow cooling conditions. The corresponding micrograph is given in Fig. 9b.
Comparing the SEM-micrographs in Fig. 9 it can be seen, that the significantly less “needle-like phase” is formed, once the cooling rate is increased. This is a hint that the “needle-like” phase in not at high-temperate stable phase but is most likely stabilized during cooling.

J Therm Spray Tech; Mikulla et. al. 2019, https://doi.org/10.1007/s11666-019-00951-4

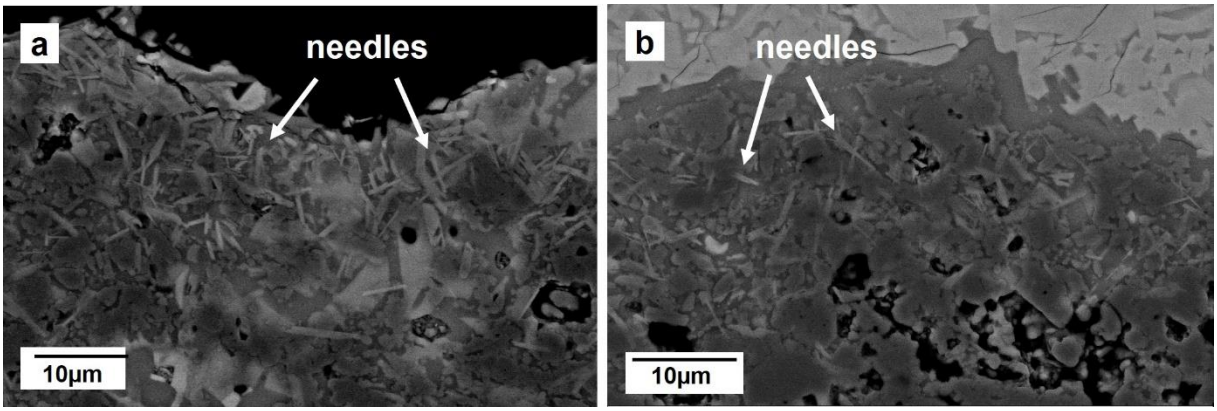

Figure 9: SEM-micrographs of SPS-alumina with CMAS2 after 5h at 1250°C with slow cooling of 10K/min (left) and rapid cooling or quenching (right) with ventilated ambient air.

Figure 10 shows SEM micrographs of the7YSZ/alumina substrate interface under a SPS coating (a) and 7YSZ columnar tips at the Al_2O_3/7YSZ interface under a crack of the SHVOF-coating (b) after 5 h infiltration with CMAS2.
With SPS alumina topcoat infiltrated strongly, the inter-columnar gaps of the 7YSZ are also infiltrated with CMAS; moreover the columns under the SPS-Al_2O_3 are detached from the substrate due to the reaction of CMAS with the alumina substrate (Fig. 10a).
Figure 10b shows the infiltrated upper part of 7YSZ columns lying under a CMAS2 infiltrated crack of the SHVOF- Al_2O_3 coating. Both the inter- and intra-columnar gaps of the 7YSZ are found to be infiltrated with CMAS. The column tips of the 7YSZ partly react with CMAS; losing the most of their original structure and forming a phase with globular shapes [6]. Since the focus of this study is the sacrificial coating, this reaction of the 7YSZ is not further studied and discussed.

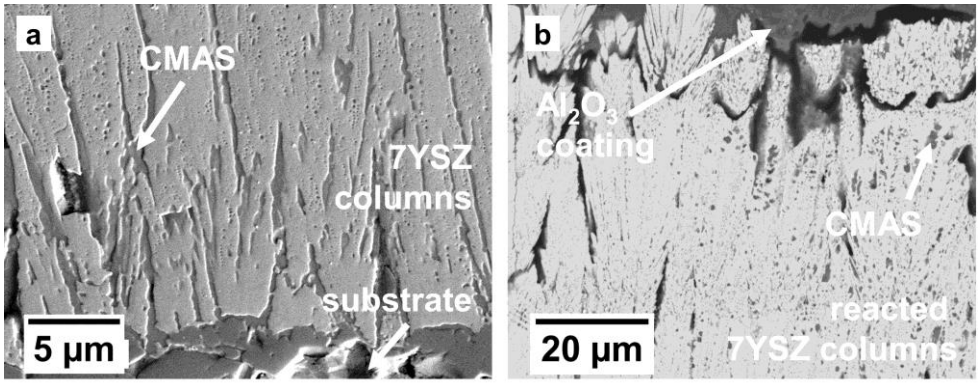

Figure 10: (a) Infiltrated and reacted 7YSZ columns under a SPS-coating at the substrate interface (b) infiltrated and reacted 7YSZ column tips located under a crack in the SHVOF-coating, both after CMAS2 infiltration 5 h @ 1250°C.

Chemical Compositions of Reaction Products in Infiltrated Al_2O_3 Coatings via EDS-Measurements

All the short-term infiltration experiments reveal the initial stages of the reaction where several new phases tend to form and could not be distinguishable explicitly due to their smaller grain sizes. Once the infiltration time extends to 5h, the reaction products could be identified clearly by using EDS spot analysis coupled with the XRD shown in Fig. 4. EDS

spot measurements on the respective phases with respect to CMAS/VA compositions and infiltration times are given in Tables 3 to 5.

The reaction products from the CMAS/VA and alumina coatings are determined by combining the XRD analysis of the powder mixtures (Fig. 4), with the chemical composition of a specific phase from the EDS spot measurements (Tab. 3 - 5).
As these reaction phases have a broad range of stoichiometry, the actual composition measured by EDS can slightly differ from the stoichiometry identified in the XRD patterns.

The following reaction products are identified during infiltration tests:

- Anorthite ($CaAl_2Si_2O_8$) phase is formed in all the studied cases as it can be seen in Fig. 5 to 8. Its composition has changed slightly with respect to the time especially in Al_2O_3 and CaO contents. Furthermore, small contents of MgO and FeO were found within it, as shown in tables 3-5. Pure anorthite only contains Al_2O_3, CaO and SiO_2; however a limited solubility of MgO and FeO is still possible. With longer annealing time the fraction of these two oxides decreased (Tab.3+4 SPS coatings 5 min and 5h). It probably diffused out of the anorthite grains and immigrated into the residue.

- Spinel ($MgAl_{2-x}Fe_xO_4$) formed in SHVOF-layers with all three different deposits after 5 h infiltration. This phase was identified at the interface between the Al_2O_3 coating and the CMAS/VA, with a layer of anorthite separating it from the deposit (Fig. 8 d,e,f). In case of CMAS2, between the anorthite and spinel, a reaction front was found which consists of MgO and FeO, but also still SiO_2 and CaO in concentrations of 5 to 7 mol.-% (Fig. 8e).
In SPS-coatings, a continuous layer of spinel forms only with CMAS1 at short- and long-term infiltration (Fig.5d + 7d), while with IVA (Fig.7c+f) spinel forms only locally and not through the entire TBC-CMAS interface. Spinel peaks are also identified in the XRD pattern of the Al_2O_3-CMAS-powder mixture (Fig 6). $MgAl_2O_4$ (spinel) is generally found when Al_2O_3 reacts with CMAS, as reported in literature [17, 18].
- Pseudobrookite ($Fe_{2-x}Ti_xO_3$) is formed for both SPS- and SHVOF-coating after annealing with Iceland volcanic ash due to the increased TiO_2 content of the ash (Fig.6c+f and Fig.8c+f). It is located in the left-over glass or in the cracks of the SHVOF-coating. They are of two different shapes, one being angular with a higher TiO_2 content of approximately 35 mol.-% and one rather round with lower TiO_2 and higher FeO of 75-80 mol.-%. Both also contain Al_2O_3. Pseudobrookite peaks are also identified in the XRD pattern of the Al_2O_3-IVA-powder mixture (Fig. 4) Pseudobrookite was found also in other studies when Al_2O_3 reacted with Iceland volcanic ash [14].

Two other phases were found only in the SPS Al_2O_3 coatings after 5 h infiltration with CMAS2: gehlenite ($Ca_2Al_2SiO_7$) and a “needle-like” structure phase (Fig.7 b and Fig. 7e), containing mainly Al_2O_3 SiO_2 and CaO, as well as MgO, FeO and TiO_2 (between 1.9 and 6.0 mol.-%). The precise determination of the chemical composition with EDS-spot measurement of this “needle-phase” is quite difficult because of its smaller size. The X-ray signals used for EDS-measurements come from an area that is at least 1 µm in diameter and around 1.5 µm in depth. As the needles are embedded in anorthite, the contents of MgO, FeO and TiO_2 could be probably much higher. In order to identify this “needle-like” structure phase, TEM examinations are necessary. The formation of this phase is linked probably to the specific microstructure that causes a certain relation of the available Al_2O_3 from the coating and the

available molten CMAS, as well as to the cooling conditions during the infiltration experiment (as seen in Fig.9).

*Table 3: Chemical composition of reaction products in the Al_2O_3 suspension sprayed coatings infiltrated with **CMAS1**, estimated by EDS spot measurements*

Possible phase	Phase abbreviation	Al_2O_3 coating / Infiltration time	Chemical composition [mol.-%] estimated by EDS spot measurements					
			$AlO_{1.5}$	SiO_2	CaO	MgO	FeO	TiO_2
Anorthite	An	SPS 5min	38.5	37.7	19.5	2.4	1.8	
		SPS 5h	38.4	40.1	19.9		1.5	
		SHVOF 5h	34.9	37.7	23.7	0.6	3.1	
Spinel	Sp	SPS 5min	49.5	2.4	1.1	29.3	17.8	
		SPS 5h	60.1			29.9	10.0	
		SHVOF 5h	64.2			26.2	9.7	
CMAS/residue	res	SPS 5min	16.4	37.2	22.4	13.1	9.0	1.9
		SPS 5h	36.0	11.2	14.1	12.4	23.5	2.9
		SHVOF 5h	12.5	35.4	26.6	10.3	13.2	2.0

*Table 4: Chemical composition of reaction products in the Al_2O_3 suspension sprayed coatings infiltrated with **CMAS2**, estimated by EDS spot measurements*

Possible phase	Phase abbreviation	Al_2O_3 coating / Infiltration time	Chemical composition [mol.-%] estimated by EDS spot measurements					
			$AlO_{1.5}$	SiO_2	CaO	MgO	FeO	TiO_2
Anorthite	An	SPS 5min	42.1	35.5	18.5	1.3	2.7	
		SPS 5h	39.7	38.2	20.6	0.6	0.9	
		SHVOF 5h	35.6	39.0	24.4		1.0	
Gehlenite	Ge	SPS 5h	39.9	19.9	36.3	2.1	1.9	
"needle-like" phase	needles	SPS 5h	69.6	8.3	11.6	3.5	5.1	1.9
		SPS 5h	71.5	6.1	10.4	3.7	6.0	2.2
		SPS 5h quench	70.9	10.0	8.5	5.6	3.1	1.8
		SPS 5h quench	78.6	4.1	7.6	3.4	4.0	2.3
Spinel	Sp	SHVOF 5h	77.2			18.1	4.8	
Reaction-front	reac-f	SHVOF 5h	60.5	7.3	5.0	21.5	5.6	
CMAS/residue	res	SPS 5min	21.3	31.7	33.8	4.7	6.6	1.9
		SPS 5h	44.1	14.8	14.8	9.5	15.9	0.9
		SHVOF 5h	18.8	36.9	31.8	9.1	2.1	1.3

*Table 5: Chemical composition of reaction products in the Al_2O_3 suspension sprayed coatings infiltrated with **IVA**, estimated by EDS spot measurements*

Possible phase	Phase abbreviation	Al_2O_3 coating / Infiltration time	Chemical composition [mol.-%] estimated by EDS spot measurements					
			$AlO_{1.5}$	SiO_2	CaO	MgO	FeO	TiO_2
Anorthite	An	SPS 5h	36.7	47.5	11.9	1.7	1.4	0.9
		SHVOF 5h	23.4	58.6	12.6	1.7	2.9	0.7
Spinel	Sp	SPS 5h	62.3			22.9	14.0	0.7
		SHVOF 5h	59.2			20.4	19.8	0.6
Pseudobrookite (angular shape)	Ps	SPS 5h	20.5			2.6	42.6	34.2
		SHVOF 5h	5.7	1.2		2.4	54.9	35.8
Pseudobrookite (round shape)		SPS 10h	13.9			4.4	75.1	6.6
		SHVOF 5h	3.6			5.5	81.3	9.6
VA/residue	res	SPS 5min	22.6	55.2	7.2	6.3	6.3	2.4

J Therm Spray Tech; Mikulla et. al. 2019, https://doi.org/10.1007/s11666-019-00951-4

Discussion

Factors Influencing the Infiltration Behavior of SPS- and SHVOF-Al_2O_3 Coatings

Infiltration behavior with respect to the suspension sprayed coating microstructure

The microstructure and especially the porosity of the alumina coatings have played a key role on the CMAS infiltration kinetics.
Figure 11 shows EDS mappings of the Si-element for SPS after 1h infiltration (a+b) and for SHVOF after 5 h (c+d) with IVA. The SPS coating and the underlying YSZ columns are strongly infiltrated. For the SHVOF-coating after 5 h infiltration however, Si from the volcanic ash can only be detected in the small reaction layer, the crack and the underlying 7YSZ layer, whereas the defect-free areas of the SHVOF layer are barely infiltrated.

The highly porous SPS-coating (~30%) is infiltrated faster than the dense SHVOF-coating (~4% porosity) and undergoes a vigorous reaction allowing the formation of different reaction products in the infiltrated areas of the coating. Since the porosity in the SPS-coating is irregular, the infiltration is, as a consequence, inhomogeneous.
Nevertheless, the presence of local distributed cracks in the SHVOF coating can be detrimental for the coating resistance, because they facilitate the local infiltration of CMAS deeper into the Al2O3 coatings until reaching even the sub-adjacent 7YSZ layer and infiltrating it entirely, as descripted in the previous study [6].

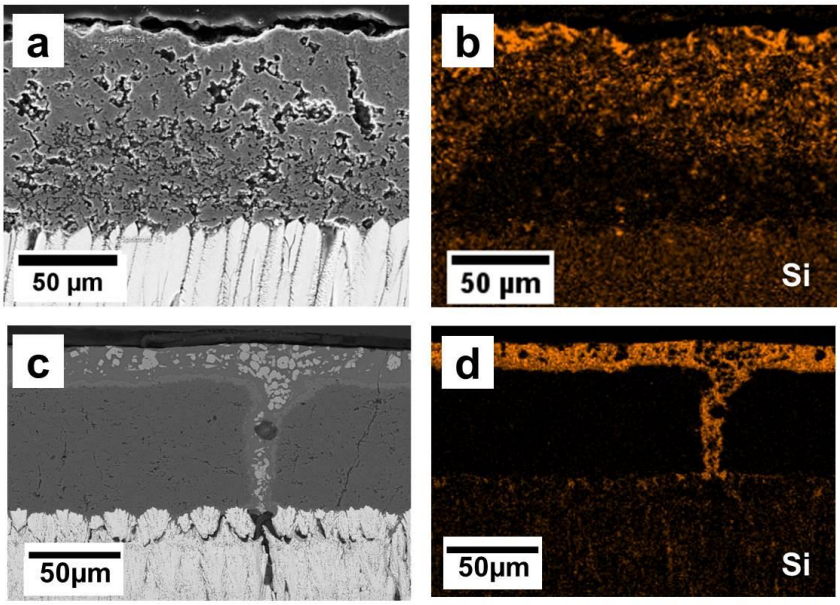

Figure 11: SEM-micrographs and corresponding EDS mapping for IVA infiltrated SPS-alumina coating after 1h (a+b) and SHVOF-alumina coating after 5 h (c+d)

J Therm Spray Tech; Mikulla et. al. 2019, https://doi.org/10.1007/s11666-019-00951-4

Infiltration behavior with respect to the chemical composition of CMAS

Apart from the microstructure of the alumina sprayed coating, the infiltration behavior of the CMAS was also influenced by the chemical composition of the applied deposit.
It is well known that the viscosity of a siliceous melt strongly depends on its chemical composition. Especially the CaO/SiO_2 ratio would give a trend in the viscosity changes, because a higher Ca/Si ratio predicts the lower viscosity. Consequently, in this study the measured values given in Table 2 strengthen this theory, too.
Due to its higher $CaO/CaSO_4$ and lower SiO_2 content, CMAS2 has a lower viscosity of 4.0 Pa·s compared to CMAS1 with 6.9 Pa·s (see also Tab.2). This drop in the viscosity explains the aggressive infiltration behavior of CMAS 2 in pores and gaps compared to the more viscous CMAS1.
A comparison of SPS-coatings exposed to CMAS1 and CMAS2 for 5 h shows a different infiltration depth (Fig.7a and b). CMAS1 infiltrated between 15-25 µm deep, whereas CMAS2 reached a depth between 20 µm and 90 µm down to the 7YSZ layer.
However, other factors apart from the viscosity must determine the infiltration kinetics, since the highly viscous IVA (251 Pa·s) infiltrated the same microstructure stronger than the less viscous CMAS 2 (4.0 Pa·s), as seen in Fig.7 b and c. To understand this deviation, the reaction kinetics and products must be taken in account, which is done later in the discussion.
The role of porosity in inhibiting the CMAS infiltration in SPS-coatings was found to be a straightforward logic, i.e. the higher the porosity the larger the CMAS attack. However, it is found out in a recent study [23] that the erosion resistance of these infiltrated coatings is reversed, where heavily infiltrated SPS alumina coatings were showing higher erosion resistance compared to a less infiltrated alumina coatings.

Reaction Kinetics and Layers

Reaction kinetics with respect to the microstructure of the alumina coatings

A clear difference in the reaction products is observed between alumina-CMAS powder mixture (reaction products identified by XRD analysis), and infiltrated SPS-Al_2O_3 and SHVOF-Al_2O_3 coatings (reaction products determined by EDS analysis). It reveals the fact that the coating microstructure plays a key role in defining the reaction products by influencing the solvent-solute-ratio. In the infiltration experiments, the alumina coating dissolved into the infiltrated CMAS and enriched with extra alumina. With increasing infiltration time, the chemical composition of the CMAS has changed significantly due to the alumina diffusion from the coating into the melt. This change in melt composition depended on how much solvent (the CMAS melt) was available in relation to the solute (here alumina or other already precipitated phases).
In case of the powder mixture, solvent and solute were well mixed, with a slight excess of CMAS concentration. This allowed the formation of anorthite, but also gehlenite, pseudobrookite and spinel which ensured enough solute/solvent ratios for the reaction products. As the pseudobrookite requires significant amounts of TiO_2 and FeO, it re-precipitated mainly in the left-over residue where there is enough solvent. The present study clearly indicates that powder experiments may give some useful information on possible phases and the reaction kinetics, but results can considerably deviate from the reactions between a real coating and a deposit.

J Therm Spray Tech; Mikulla et. al. 2019, https://doi.org/10.1007/s11666-019-00951-4

In case of the SPS coating, for all the infiltration cases, the melt has infiltrated into the smaller pores and was surrounded by enough alumina coating. Hence, local melt composition is enriched with the alumina. When being infiltrated with CMAS1 and IVA the reaction phases in the SPS-coating are similar to those in SHVOF.
Two phases, namely gehlenite and the 'needle-like phases', are only formed in case of CMAS2 infiltration in the SPS coating. Gehlenite crystals were formed only after the 5 h infiltration and merely in larger gaps. Its formation seems to require less alumina than anorthite and more CaO; once the melt forms anorthite, the rest glass which contains all the other oxides would crystallize into gehlenite phase upon slow isothermal cooling. As previously mentioned, the 5 min infiltration tests contain quick quenching, whereas the 5 h experiments were slowly, isothermally cooled (10 K/min) which would allow the separation of phases. That can be the main reason for the absence of gehlenite phase in case of the 5 min experiment. TiO_2 and FeO appeared in the "needle-like" phases (Table 4) of SPS infiltrated for 5 h @ 1250 °C. The absence of TiO_2 in both anorthite and gehlenite and higher presence of FeO in needle-like phase can be pointed out from Table 4. It is known from literature that TiO_2 reacts with FeO to form pseudobrookite. As we see from the needle-like phase, in case of SPS alumina after 5 h, there exists a tendency that TiO_2 –FeO rich phase containing all other elements would form pseudobrookite upon long-term annealing.

For the same CMAS2 case, spinel formation in SHVOF-coating was a direct evidence of coating microstructure influence, where dense alumina offers resistance to the CMAS infiltration and allowed enough time which triggers the reaction with FeO and MgO.

In case of CMAS1, the microstructure did not play a significant role, as both SPS and SHVOF have formed anorthite and spinel as reaction products. This can be explained by the increased viscosity of CMAS1 that slowed down infiltration kinetics and by the lower TiO_2 content, thus the formation of (Mg,Al)-spinel or (Mg, Fe)Al-spinel phases is favorized instead the reaction of FeO with TiO2 to result in pseudobrookite reaction product.
In contrast, the high viscous glass IVA, which should allow more reaction time compared to that of CMAS2/CMAS1, could not form a continuous spinel layer as a reaction product on the SPS coating. This can only be explained on the basis of influence of chemistry as described in the following section.

<u>Reaction kinetics with respect to the chemical composition of the CMAS deposit</u>

Alumina coating has produced different reaction products depending on the local chemical composition of the CMAS/VA melts. Especially both CMAS compositions differ in their CaO content. They both have reacted vigorously with the alumina and formed almost same products except gehlenite.

The gehlenite phase could be only found in the CMAS2-Al_2O_3 powder mixture and in the SPS-coating for CMAS2. This can be explained considering the ternary phase diagram of $AlO_{3/2}$-SiO_2-CaO at an isothermal cut of 1300 °C (Fig. 12). The compositions of CMAS2 (red circle), CMAS1 (blue triangle, also used in[18]) and IVA (green square) are marked in the phase diagram by using the normalized Al_2O_3-SiO_2-CaO fractions of the two CMAS while eliminating FeO, MgO and TiO_2 fractions. During the infiltration, the CMAS/VA melt is enriched with Al_2O_3 (from the coating), moving the CMAS compositions along the red, blue or green line towards the alumina. In case of CMAS1, the chemical composition lies in the phase field of anorthite and with the extra alumina intake from the dissolved coating it still

precipitates as ‘anorthite’ (blue dashed line). Contrarily, the CMAS2 melt composition (and its position in the phase diagram) is different due to the increased calcia content. As a consequence, when CMAS2 is enriched with alumina, the melt composition (red circle) will not pass through the ‘anorthite point’ but move through the line, where both anorthite and gehlenite will be re-precipitated (red line). Furthermore, the viscosity of CMAS2 is lower compared to that of CMAS 1 (table 2), which can be one factor explaining the absence of sealing spinel layer on SPS coatings. Due to its slightly higher viscosity, the CMAS1 infiltrates the SPS-coating a bit slower than the CMAS2 giving enough time to react and form spinel.

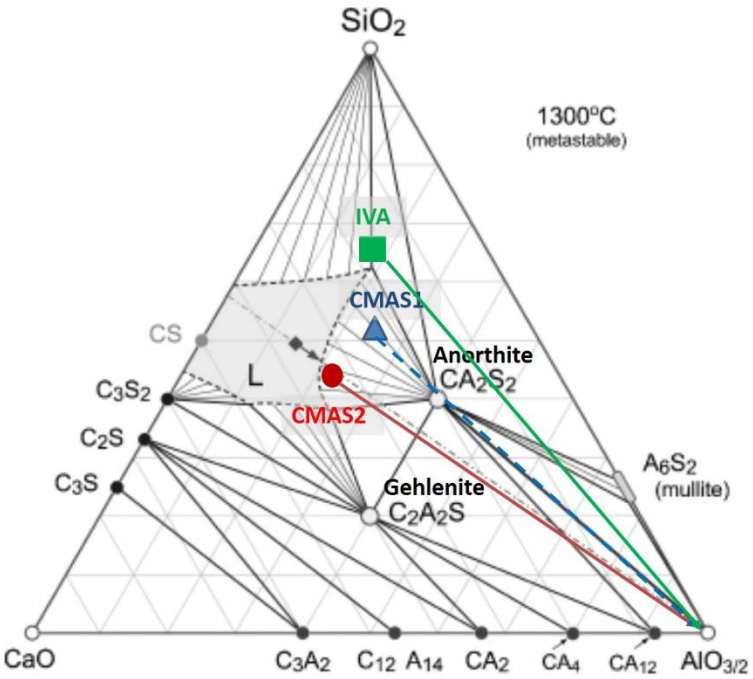

Figure 12: Ternary phase diagram $AlO_{1.5}$-SiO_2-CaO, metastable isothermal cross section at 1300°C [24] based on [25] (Fig. 630), the relative composition of CMAS1(blue triangle), CMAS2 (red circle) and IVA (green square) , colored lines indicating the composition of each CMAS/VA with increasing Al_2O_3 content

However, the formation of a sealing spinel layer is not only linked to the viscosity of the melt, as it can be seen in case of the island volcanic ash. Although its viscosity is two orders of magnitudes higher than the both CMAS compositions, it has infiltrated the whole SPS-alumina coating. It is known from the literature, that FeO is very important for the formation of (Fe,Mg) Al-spinel layer [18]. At the same time,TiO_2 reacts with FeO to form pseudobrookite [18]. In the IVA melt with its higher TiO_2 content, it has formed iron-containing pseudobrookite as shown in Fig.6 f and 8 f. This reaction has reduced the amount of free FeO available for the spinel formation. This shows that viscosity is not only determining infiltration behavior but also reaction kinetics plays a greater role in defining the reaction products.

<u>Reaction layer growth and stability:</u>
The formation of a high temperature stable, slowly growing, and well adherent sealing reaction layer against CMAS attack (crystalline phases) is the key in defining the protective nature of any sacrificial layer, such as Al_2O_3, that are used on top of TBCs.

J Therm Spray Tech; Mikulla et. al. 2019, https://doi.org/10.1007/s11666-019-00951-4

Considering the SEM micrographs of the infiltrated SPS and SHVOF layers, it can be seen that uniform reaction layers were formed on top of the SHVOF-Al_2O_3 coating for all three deposits (CMAS1, CMAS2, IVA, Fig. 6 and Fig. 8). For SPS-Al_2O_3 a uniform layer was formed only in case of CMAS1 (Fig.5a,c + 7a,c).
The protective reaction layer consist mainly of (Fe,Mg)Al-spinel and all the other products were either formed during cooling or discontinuously offering no protection against infiltration. This is in accordance with previous studies with EB-PVD alumina coatings[18], where (Fe,Mg) Al-spinel was the only reaction product that could seal smaller gaps against infiltration.

The thickness of the reaction layer with respect to the annealing times for SHVOF alumina is drawn in Fig.13.
After short term infiltration, the reaction layer was found to be between 1.2 ± 0.3 µm thick for CMAS1, 1.4 ± 0.4 µm for CMAS2 and 1.8 ± 0.4 µm for IVA. The reaction layer thickness increased continuously up to 3.7 ± 0.8 µm for IVA, 5.5 ± 0.5 µm for CMAS2 and 7.0 ± 1.4µm for CMAS1 after 10 h. For both CMAS compositions, the kinetics show a linear growth whereas for IVA experiences a parabolic growth. It is observed that the growth kinetics is higher for CMAS1, whereas IVA exhibited the least. There is no comparable trend found on the basis of viscosity as the CMAS2 exhibits the least viscosity and its layer thickness stays in the center of CMAS1 and IVA. However, a conclusion can be drawn that the chemical composition of the melt defines the spinel layer growth here.

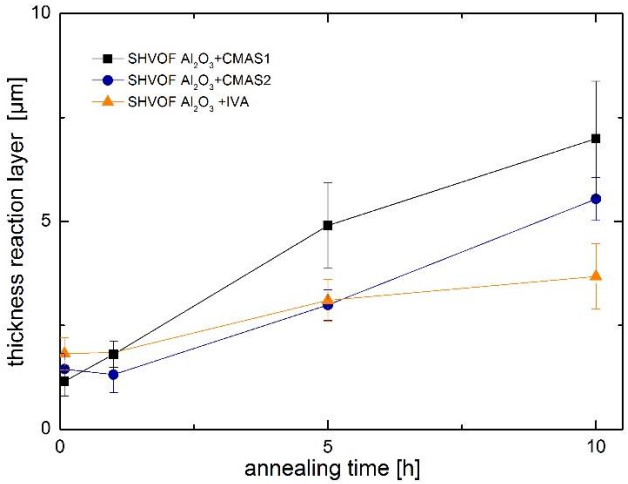

Figure 13: Thickness of the reaction layer at different annealing times for SHVOF-Al_2O_3 coatings with CMAS/VA deposits

As for the available data, a comparison is drawn between different coating microstructures of alumina coatings obtained by SPS, SHVOF and EB-PVD methods. Figure 14 shows the reaction layer thickness of SHVOF-, SPS- and EB-PVD alumina coatings after infiltration with in the time frame of 5 min to 10 h with CMAS1. The data for the 110 µm thick EB-PVD alumina coating is taken from previous studies [18], in which the infiltration experiments were performed and analyzed under same conditions.

J Therm Spray Tech; Mikulla et. al. 2019, https://doi.org/10.1007/s11666-019-00951-4

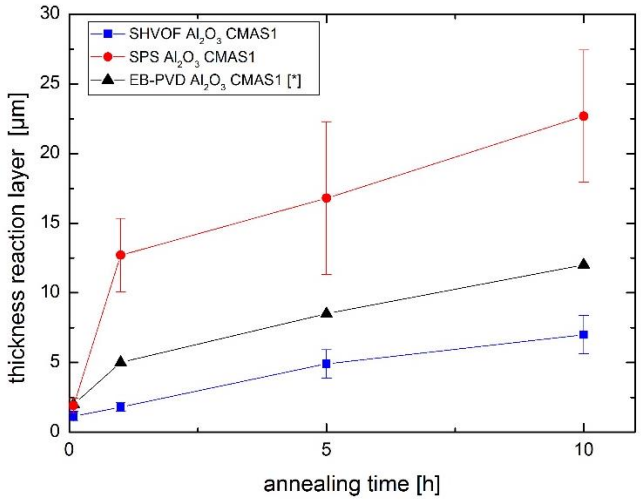

*Figure 14: Thickness of the reaction layer at different annealing times for SHVOF-, SPS- and EB-PVD-Al_2O_3 [*ref]: [18] coatings after infiltration with CMAS1 at 1250°C*

During the initial stage, at annealing times up to 1 h, the reaction layer exhibits different kinetics due to the different microstructure and porosity. The highly-porous SPS coating is infiltrated easier and forms a thicker reaction layer of around 12 µm than the dense SHVOF-coating, which has a thinner reaction layer of only 2 µm after the same annealing time. The formation of a thicker reaction layer in the SPS coating implied a higher consumption of the alumina during reaction with CMAS. After 1 h, when already uniform reaction layers have formed for both the SPS and SHVOF-coating, the growth of the reaction layers slows down and continues at a relatively constant rate. Although the increase rate between 1 h and 10 h for the three coatings is closer than in the initial stage, the reaction layer of the SPS-coating is still growing faster than SHVOF- and EB-PVD coating. The difference between the three curves indicates the effect of the microstructure on the formation of the reaction layer. The highly porous SPS-coating forms the thickest layer when reacting with CMAS1, more than 23.0 ± 4.7 µm followed by the feathery EB-PVD-columns, with 12.0 µm. In the dense SHVOF-coating the reaction layer was after 10 h of about only 7.0 ±1.4 µm, indicating the slowest reaction, i.e. the higher the porosity higher the thickness of the reaction layer.

Conclusions

Al_2O_3 sprayed coatings with defined coating microstructures and porosity levels were produced by two different suspension spraying methods on top of EB-PVD 7YSZ layers. Porous alumina coatings with about 30 % porosity were obtained by SPS, whereas a very dense structure with porosity content below 4 % was obtained by SHVOF.
Infiltration experiments between 5 min and 10h at 1250°C were performed with two artificial CMAS deposits and one natural volcanic ash.
The response and the effectiveness of the sacrificial alumina suspension sprayed coatings against CMAS infiltration were influenced by the coating microstructure and by the chemical composition of the deposit.
From the performed experiments, following conclusions on the reaction products formation can be drawn:

J Therm Spray Tech; Mikulla et. al. 2019, https://doi.org/10.1007/s11666-019-00951-4

- The reaction products anorthite ($CaAl_2Si_2O_8$), gehlenite ($Ca_2Al_2SiO_7$), alumina containing pseudobrookite ($Al_yFe_{2-x-y}Ti_xO_3$) and a 'needle-like' phase ($(Al,Ca,Si, Fe,Mg)O_x$) were found in both alumina SPS and SHVOF coating microstructures; these products did not resulted in continuous, sealing layers to stop further CMAS infiltration.
- Uniform spinel layers ($MgAl_{2-x}Fe_xO_4$) act as an efficient, slow growing barrier against CMAS infiltration. For SHVOF coatings, they are formed with all three CMAS/VAs due to its dense structure, whereas in case of SPS alumina, it was only formed with CMAS1, which is sufficiently viscous and supplies enough FeO for its formation.
  A sufficient supply of FeO by the melt was found to be crucial for the formation of the spinel phase. For deposits/melts with high TiO_2 content like IVA, the amount of FeO is reduced by its incorporation into the emerging pseudobrookite phase
- The homogeneous CMAS-Alumina powder mixtures have exhibited slightly different reaction products than in the coated samples, as the local solute-solvent-ratio differs from the ratio in a coating with microstructure.

The coating microstructures strongly influenced the infiltration behavior of the CMAS melt. Highly porous SPS alumina coatings were infiltrated faster and have reacted stronger as they offer a higher specific contact surface area with the CMAS. From all the CMAS compositions tested, only CMAS1 could form a continuous spinel layer irrespective of porosities both in SPS and SHVOF, i.e. chemical reactivity can overcome the porosity effect. For CMAS2 and IVA a continuous protective spinel layer could not be produced in the SPS coating mostly because of their differences in the chemical composition and viscosity.
The SHVOF-coatings have shown a promising CMAS sealing, infiltration hindering behavior due to the formation of uniform, thin spinel layers, although the local-distributed through-thickness cracks have proven to be weak areas allowing the localized infiltration of the CMAS. Further optimization of the coating process is needed to improve the consistency of the coating when exposed to CMAS mitigation and elevated temperatures.

Acknowledgments
The authors express their gratitude to J. Brien, A. Handwerk and D. Peters from DLR Cologne for producing of the EB-PVD 7YSZ layers, as well as for technical support and advisory. The work was performed in the Framework of the Research Project DFG No. SCHU 1372/5 1, LE1373/34-1 funded by DFG-Deutsche Forschungsgemeinschaft (German Research Foundation). The authors acknowledge the financial support.

References

1. D.R. Clarke, M. Oechsner, and N.P. Padture, Thermal-barrier coatings for more efficient gas-turbine engines. *Mrs Bull*, 2012, **37**(10), p 891-902
2. C.G. Levi, Emerging materials and processes for thermal barrier systems. *Curr Opin Solid St M*, 2004, **8**(1), p 77-91
3. A.F. Renteria, B. Saruhan, U. Schulz, H.J. Raetzer-Scheibe, J. Haug, and A. Wiedemann, Effect of morphology on thermal conductivity of EB-PVD PYSZ TBCs. *Surf Coat Tech*, 2006, **201**(6), p 2611-2620
4. S. Sampath, U. Schulz, M.O. Jarligo, and S. Kuroda, Processing science of advanced thermal-barrier systems. *Mrs Bull*, 2012, **37**(10), p 903-910
5. R. Naraparaju, U. Schulz, P. Mechnich, P. Döbber, and F. Seidel, Degradation study of 7wt.% yttria stabilised zirconia (7YSZ) thermal barrier coatings on aero-engine combustion chamber

parts due to infiltration by different CaO–MgO–Al2O3–SiO2 variants. *Surface and Coatings Technology*, 2014, **260**, p 73-81
6. R. Naraparaju, M. Huttermann, U. Schulz, and P. Mechnich, Tailoring the EB-PVD columnar microstructure to mitigate the infiltration of CMAS in 7YSZ thermal barrier coatings. *Journal of the European Ceramic Society*, 2017, **37**(1), p 261-270
7. R. Naraparaju, P. Mechnich, U. Schulz, and G.C.M. Rodriguez, The Accelerating Effect of CaSO4 Within CMAS (CaO-MgO-Al2O3-SiO2) and Its Effect on the Infiltration Behavior in EB-PVD 7YSZ. *Journal of the American Ceramic Society*, 2016, **99**(4), p 1398-1403
8. C.G. Levi, J.W. Hutchinson, M.H. Vidal-Setif, and C.A. Johnson, Environmental degradation of thermal-barrier coatings by molten deposits. *Mrs Bull*, 2012, **37**(10), p 932-941
9. R. Naraparaju, J.J.G. Chavez, P. Niemeyer, K.U. Hess, W.J. Song, D.B. Dingwell, S. Lokachari, C.V. Ramana, and U. Schulz, Estimation of CMAS infiltration depth in EB-PVD TBCs: A new constraint model supported with experimental approach. *Journal of the European Ceramic Society*, 2019, **39**(9), p 2936-2945
10. R. Naraparaju, J.J.G. Chavez, U. Schulz, and C.V. Ramana, Interaction and infiltration behavior of Eyjafjallajokull, Sakurajima volcanic ashes and a synthetic CMAS containing FeO with/in EB-PVD ZrO2-65 wt% Y-2 O-3 coating at high temperature. *Acta Mater*, 2017, **136**, p 164-180
11. M.A. Rivera-Gil, J. Gomez-Chavez, C.V. Ramana, R. Naraparaju, U. Schulz, and J. Munoz Saldana, High Temperature Interaction of Volcanic Ashes with 7YSZ TBC´s produced by APS: Infiltration behavior and phase stability. *Surface and Coatings Technology*, 2019, **378**, p 124915
12. W.J. Song, Y. Lavallee, K.U. Hess, U. Kueppers, C. Cimarelli, and D.B. Dingwell, Volcanic ash melting under conditions relevant to ash turbine interactions. *Nature Communications*, 2016, **7**, p 10795
13. P. Mohan, B. Yao, T. Patterson, and Y.H. Sohn, Electrophoretically deposited alumina as protective overlay for thermal barrier coatings against CMAS degradation. *Surface and Coatings Technology*, 2009, **204**(6), p 797-801
14. S. Kramer, J. Yang, and C.G. Levi, Infiltration-inhibiting reaction of gadolinium zirconate thermal barrier coatings with CMAS melts. *Journal of the American Ceramic Society*, 2008, **91**(2), p 576-583
15. U. Schulz and W. Braue, Degradation of La2Zr2O7 and other novel EB-PVD thermal barrier coatings by CIVIAS (CaO-MgO-Al2O3-SiO2) and volcanic ash deposits. *Surf Coat Tech*, 2013, **235**, p 165-173
16. A.K. Rai, R.S. Bhattacharya, D.E. Wolfe, and T.J. Eden, CMAS-Resistant Thermal Barrier Coatings (TBC). *International Journal of Applied Ceramic Technology*, 2010, **7**(5), p 662-674
17. X.-f. Zhang, K.-s. Zhou, W. Xu, B.-y. Chen, J.-b. Song, and M. Liu, In situ synthesis of α-alumina layer on thermal barrier coating for protection against CMAS (CaO–MgO–Al2O3–SiO2) corrosion. *Surface and Coatings Technology*, 2015, **261**, p 54-59
18. R. Naraparaju, R.P. Pubbysetty, P. Mechnich, and U. Schulz, EB-PVD alumina (Al2O3) as a top coat on 7YSZ TBCs against CMAS/VA infiltration: Deposition and reaction mechanisms. *Journal of the European Ceramic Society*, 2018, **38**(9), p 3333-3346
19. L.-M. Berger, F.-L. Toma, and A. Potthoff, Thermal Spraying with Suspensions-An Economic Spray Process. *Thermal Spray Bulletin*, 2013, **6**(2), p 98-101
20. F.L. Toma, A. Potthoff, L.M. Berger, and C. Leyens, Demands, Potentials, and Economic Aspects of Thermal Spraying with Suspensions: A Critical Review. *J Therm Spray Techn*, 2015, **24**(7), p 1143-1152
21. A. Potthoff, R. Kratzsch, M. Barbosa, N. Kulissa, O. Kunze, and F.L. Toma, Development and Application of Binary Suspensions in the Ternary System Cr2O3-TiO2-Al2O3 for S-HVOF Spraying. *J Therm Spray Techn*, 2018, **27**(4), p 710-717
22. M. Barbosa, et al. Suspension Sprayed YSZ Thermal Barrier Coatings: Road to Industrial Application. *ITSC 2018—Proceed. Intern. Therm. Spray Conf.* . K.B. F. Azarmi, T. Eden, T. Hussain, Y.-C. Lau, H. Li, K. Shinoda, F.-L. Toma, J. Veilleux (Orlando, Florida, USA), ASM Int. 2018 2018 p 113- 119

23. L. Steinberg, C. Mikulla, R. Naraparaju, F.-L. Toma, H. Großmann, U. Schulz, and C. Leyens, Erosion resistance of CMAS infiltrated sacrificial suspension sprayed alumina top layer on EB-PVD 7YSZ coatings. *Wear*, 2019, **438-439**, p 203064
24. S. Krämer, J. Yang, C.G. Levi, and C.A. Johnson, Thermochemical Interaction of Thermal Barrier Coatings with Molten CaO–MgO–Al2O3–SiO2 (CMAS) Deposits. *Journal of the American Ceramic Society*, 2006, **89**(10), p 3167-3175
25. E.M. Levin, C.R. Robbins, and H.F. McMurdie, *Phase Diagrams for Ceramists*, vol. I, The American Ceramic Society, Columbus, OH, 1964, p 210, 219, 246